Proc. of the European Safety and Reliability Conference (ESREL 2026)
Edited by José C. Matos, Paulo B. Lourenço, Michael Beer, Daniel Oliveira, Edoardo Patelli, Hélder S. Sousa, Rui A. Silva and Monica Santamaria

doi: 10.3850/ESREL2026061419_esrel26-p26377-cd

Towards accurate predictive modelling of liquid hydrogen pool dynamics

Davide Rescigno

Department of Mechanical and Industrial Engineering, Norwegian University of Science and Technology, Richard Birkelands vei 2B, 7034 Trondheim, Norway. E-mail: davide.rescigno@ntnu.no

Federico Ustolin

Department of Mechanical and Industrial Engineering, Norwegian University of Science and Technology, Richard Birkelands vei 2B, 7034 Trondheim, Norway. E-mail: federico.ustolin@ntnu.no

Liquid hydrogen (LH_2) is one of the main green energy vectors currently pursued to achieve decarbonization in the maritime sector. However, its use can lead to several consequences due to loss of containment. After a leak of LH_2, a pool may form and extend the hazard time, during which the hydrogen gas, after evaporation, can encounter an ignition source. To better estimate and understand the evaporation time of a pool after its spreading, this study develops and validates a ring reduction model for simulating cryogenic pool spreading and evaporation. In the proposed model, the cryogenic liquid pool is discretized by rings, which allow for a more precise evaporation calculation and better simulate the pool spreading and shrinking. The model solves local mass and energy balances at each time step, calculating heat flux, evaporation, and accurately calculates transient ground temperature profiles. During evaporation, the radius is updated by progressively removing the outer and inner rings as their mass evaporates. This study proves that while the ring reduction model is robust, the implementation of the right heat transfer correlations for cryogenic pools is still a research gap that must be addressed to accurately replicate pool scenarios.

Keywords: safety, cryogenic fluids, liquid hydrogen, pool spreading, modelling.

1. Introduction

Liquid hydrogen (LH_2) is a flammable fluid that can lead to severe consequences. Since LH_2 is stored at cryogenic temperature, leaks from cryogenic equipment might occur (Goff *et al*. 2024). After a leak of LH_2, the fluid breaks down into droplets and is subjected to flashing (Rescigno *et al.* 2025). These droplets are subject to evaporation and might reach the ground, form a pool, and extend the hazard time. This pool is then subject to evaporation due to the temperature difference between the ground and the cryogenic liquid. The evaporated gas will then mix with the air, and if ignited, it can lead to various phenomena such as explosions, flash fire, or ignite a pool fire (Holborn *et al 2022*; Hall *et al* 2014). Additionally, given that the hydrogen boiling temperature is lower than the freezing point of oxygen, a condensed-phase explosion represents another phenomenon that must be considered (Ustolin *et al* 2022).

While the condensed-phase explosion is an important research gap, there are integral models that can simulate pool spreading. For instance, the DNV software PHAST (Witlox *et al* 2023) is able to simulate pool spreading and evaporation (PVAP model) after a discharge of various fluids. Although PHAST is not validated for the use of LH_2, it is widely used to assess pool scenarios. In PHAST, the pool evaporation is simulated while assuming a constant height. Another integral model, GASP, developed by the Health and Safety Executive (HSE) in the UK (Webber 1990), consists of a system of coupled ordinary differential equations that describe the temporal evolution of the global properties of the pool. Six primary variables are defined to represent the pool: i) radius, ii) radial velocity of the liquid at the edge, iii) liquid volume, iv) pool temperature, v) discharged liquid volume, and vi) vaporized volume. In both PHAST and GASP, the heat flux is calculated using Fourier's law of conduction (TNO 2005; Witlox *et al* 2023), assuming a constant surface contact and solving the semi-infinite solid problem.

However, assuming a constant surface may overpredict the heat flux, because LH_2 due to its cryogenic temperature can be subject to different regimes (nucleate boiling, transition, and film boiling) when it spreads on the ground. The regime depends on the temperature difference between the ground and the cryogenic fluid (Wang *et al*. 2016). During the nucleate boiling regime, the warm wall creates a local superheated liquid layer in contact with the surface, leading to vapor bubble formation (Baldwin *et al*. 2021). The bubbles then grow due to thermal diffusion and hydrodynamic instability. At higher temperature differences, a continuous vapor film forms between the pool and the ground, and heat transfer occurs mainly by convection through the film itself (Baldwin *et al*. 2021).

Other approaches, such as the LAUV model (Verfondern and Dienhart 2007) and the one adopted by (Grønli *et al* 2025), use the shallow water equations to simulate the pool spreading, where the pool height and velocity are described as functions of space and time through a system of nonlinear partial differential equations. To better evaluate the pool spreading, vaporization, and contraction, this study proposes a model where ground temperature and pool mass are functions of space and time, assuming an average pool height. The pool is discretized into concentric rings, on which local mass and energy balances are solved to calculate heat flux, transient ground temperature profiles, and evaporation rates. During evaporation, the radius of the pool is updated by progressively removing the inner and outer rings as their mass is evaporated, improving the estimation of evaporation time.

2. Methodology

2.1 Pool model with retraction

In this study, the pool is represented as an axially symmetric domain, discretized radially into concentric rings. Each ring represents a portion of the surface that is "wet" by the liquid at a different instant, and whose temperature evolves independently over time. This allows the reconstruction of the ground temperature field and the local heat flow as a function of both time and radial position. At each time step, the model solves:

- The redistribution of mass across the rings,
- The growth or contraction of the pool radius,
- The calculation of the surface temperature beneath each ring of the pool,
- The heat balance for each ring,
- The local evaporation of the liquid for each ring,
- The calculation of the average pool height.

2.1.1 Spreading law

During the growth phase, the radius of the pool is updated based on the spreading velocity linked to the average thickness of the liquid. The radial velocity u_r [m/s] is defined as per Eq. 1, adapted from (Witlox 2000):

$$u_r = \sqrt{2g\,(H - H_{min})} - CF \tag{1}$$

Where g is the acceleration due to gravity [m/s^2], H is the average thickness of the puddle [m], H_{min} is a minimum thickness threshold [m] , CF is a viscous resistance term added to account for ground friction [m/s], and calculated as per (TNO 2005). During the growing phase, the radius of the pool r [m] is updated with the correlation from (TNO 2005) for smooth subsoil (Eq.(2)):

$$\frac{dr}{dt} = u \tag{2}$$

As the radius increases, the surface of the pool is divided into N concentric rings, each defined by an inner radius and an outer radius, leading to an area A_j [m^2].

2.1.2 Ground thermal model

The terrain is modeled as a semi-infinite solid with no internal generation of thermal energy, no radial thermal gradient, and constant thermal conductivity. The ground temperature T [K] is calculated with a 1-D model, as per Eq. 3:

$$\frac{\partial^2 T}{\partial z^2} = \frac{1}{\alpha}\frac{\partial T}{\partial t} \tag{3}$$

Where z is the vertical coordinate [m], and α is the thermal diffusivity [m^2/s]. The soil is subject to a convective boundary condition upon contact with the cryogenic liquid, as per Eq. 4:

$$-k\left.\frac{\partial T}{\partial z}\right|_{z=0} = h\left(T_{fluid} - T_g(0,t)\right) \tag{4}$$

Where $T_g(0,t)$ is the ground temperature [K] at $z = 0$ and at time t, T_{fluid} is the cryogenic fluid temperature [K], h is the convective heat transfer coefficient [W/m^2·K], and k is the thermal conductivity of the ground [W/m·K]. The model assumes that the pool is at a constant temperature, T_{fluid}, namely the saturation temperature at ambient pressure, which is 20.3 K for LH_2. All thermodynamic properties in the model are derived from the CoolProp library developed by (Bell *et al.* 2014). In the proposed model, h is estimated using a boiling curve as a function of the local temperature difference between the ground and the cryogenic fluid. The boiling curve code was obtained from the study conducted by (Ustolin *et al.* 2021) and subsequently modified for the purposes of this work. For each time step and for each ring, the model calculates the appropriate boiling regime, returning h for each wet area A_j over the release time. Due to the difference between the ground temperature and LH_2, heat transfer will occur primarily via the film boiling regime, defined as per Eq. (5) (Breen and Westwater 1962):

$$q = \frac{0.37+0.28\frac{l_c}{D}}{\left(\frac{l_c\,\mu_v\,\Delta T}{\lambda_v^3\,\rho_v(\rho_l-\rho_v)\,g\,H_f'}\right)^{1/4}}\,\Delta T \tag{5}$$

Where l_c is the Laplace length [m], D refers to the pool diameter [m], μ_v is the gas dynamic viscosity [kg/m·s], ΔT is the temperature difference between the pool and the ground [K], λ_v is the vapor thermal conductivity [W/m·K], ρ_v is the gas density [kg/m^3], ρ_l is the liquid density [kg/m^3], g is the gravity constant [m/s], and H_f' is the effective latent heat of vaporization calculated as in (Ustolin *et al.* 2021).

By solving Eq. 3 and Eq. 4 for any concentric ring A_j, the ground temperature $T_{g,j}(r,z,t)$ can be calculated as per Eq. 6:

$$T_{g,j}(r,z,t) = T_i + \left(T_{fluid} - T_i\right)\left[erfc\left(\frac{z}{2\sqrt{\alpha t}}\right) - \exp\left(\frac{h_j z}{k} + \frac{h_j^2 \alpha t}{k^2}\right) erfc\left(\frac{z}{2\sqrt{\alpha t}} + \frac{h_j\sqrt{\alpha t}}{k}\right)\right] \tag{6}$$

Where T_i is the initial temperature of the soil [K], $T_{g,j}(r,z,t)$ is the temperature of the concentric ring A_j at the coordinate z and wet time t. As Eq. 6 suggests, the soil temperature in each ring depends on the elapsed time since the liquid wetted the specific region.

2.1.3 Local energy balance and pool contraction procedure

For each ring, the conductive heat flux $\dot{q}_{\mathrm{cond},j}(r,t)$ [W/m^2] from the ground to the liquid is expressed as (Eq. 7):

$$\dot{q}_{\mathrm{cond},j}(r,t) = h_j\left(T_{g,j} - T_{fluid}\right) \tag{7}$$

To obtain the outgoing heat flux ($\dot{Q}_{\mathrm{out}}$), convection with air and radiation are added to the conduction term. The heat exchange between the surface of the pool (T_{fluid}) and the ambient air is modeled as laminar flow over an isothermal plate, thus the average convection coefficient $\overline{h}_x$ [W/m^2·K] along the pool surface is assumed as per Eq. 8 (Bergman and Lavine 2018):

$$\overline{h}_x = \frac{0.664\,Re_L^{1/2}\,Pr^{1/3}k}{L} \tag{8}$$

Where $\mathrm{Re_L}$ is the Reynolds number for a laminar flow [-], Pr is the Prandtl number [-], k is the kinematic viscosity [m^2/s]. The net radiative contribution between the surface of the pool and the environment is expressed, in general terms, by Stefan-Boltzmann's law. The ground properties (e.g., the emissivity) are highlighted in Table *2*. Once the outgoing heat flux is computed, the evaporation rate of the pool mass ($\dot{m}_{ev,j}$) in any ring can be computed as per Eq. (9):

$$\dot{m}_{ev,j}(r,t) = \frac{\dot{Q}_{out,j}(r,t)}{L_v} \tag{9}$$

Where $\dot{Q}_{\text{out},j}$ is the outgoing heat flux [W] of the j-th ring, and L_v is the latent heat of vaporization [J/kg]. During the spreading phase, the total volume increases and new outer rings are created as the mass is redistributed with a uniform thickness (H), turning the mass of each ring proportional to its area. At the same time frame, the local energy balance is computed, and the evaporated mass is calculated. When the total volume decreases, the radius is not reduced kinematically but is updated by progressively removing the outer (or inner) rings (whose areas are A_j) as soon as their masses evaporate. Ultimately, the average height is calculated by considering the total volume of the pool and the updated radius.

2.4 Case study

Pool spreading simulations were carried out against the experimental data of NASA test 6 (Chirivella and Witcofski 1986). The available experimental data are outlined in *Table 1*.

Table 1. Experimental data from NASA test 6 (Chirivella and Witcofski 1986).

Parameter	NASA test 6
Mass flow rate	9.50 [kg/s]
Release duration	38.00 [s]
Impact surface	1.2 x 1.2 m metal plate, with sand surrounding it

Since the LH_2 flashing and droplet evaporation are out of the scope of this study, three mass flow rate scenarios were simulated to compare the results with the NASA test 6: case A) $\dot{m}_{LH2} = 9.5$ kg/s; case B) $\dot{m}_{LH2} = 4.75$ kg/s; case C) $\dot{m}_{LH2} = 2$ kg/s, with a spill zone (the area on the ground where the liquid is introduced into the numerical model) of 0.75 m. In the simulation, sand is considered as the impact surface, although the impact surface in the experiment comprises a 1.2 x 1.2 m metal plate and sand outside it. The main physical parameters used for the simulation are summarized in Table *2*.

Table 2. Physical parameters.

Parameter	Value	Reference
Thermal conductivity of sand	0.94 W/m·K	(Grønli, Skarsvåg, and Munkejord 2025)
Thermal diffusivity of sand	$4.88 \cdot 10^{-7}$ m²/s	(Grønli, Skarsvåg, and Munkejord 2025)
Emissivity of sand	0.9 [-]	(Bergman and Lavine 2018)
Spill zone	0.75 m	(Grønli, Skarsvåg, and Munkejord 2025)
Wind speed	2.2 m/s	(Jin *et al.* 2017)
Initial ground temperature	278.15 K	-
Ambient temperature	288.15 K	(Jin *et al.* 2017)

3. Results

Figure 1 shows the results of the pool model considering three different mass flow rates. Since discharge parameters and release height of NASA test 6 are unknown, to account for the LH_2 evaporation before ground contact, it is necessary to simulate and hypothesize different scenarios. The pool radius and height were plotted until the LH_2 mass within any ring j evaporated. As expected, the lower the mass flow rate, the smaller the maximum pool radius. While case A) greatly overpredicts the maximum pool radius, case C) slightly overpredicts the pool radius. The results warn that flashing and droplet evaporation are a non-negligible phenomenon. The results outlined in Figure 2 reveal a good agreement with the evaporation time of 5.5 s following the termination of the liquid discharge of NASA test 6. Notably, while in the case A) the pool evaporated after 11 s following valve shut-off, in the case C) the pool evaporated only after 7 s. This trend is consistent with experimental results, since a larger radius implies a larger mass and a higher thermal capacity, and thus requires a higher evaporation time. Additionally, Figure 2 points out that after 13 s the pool reaches a steady state since the rate of pool evaporation and the rate of cumulative mass addition are equal. During this phase, the pool radius increases while the pool height decreases, suggesting that during the steady state, the mass of LH_2 is distributed along the radius.

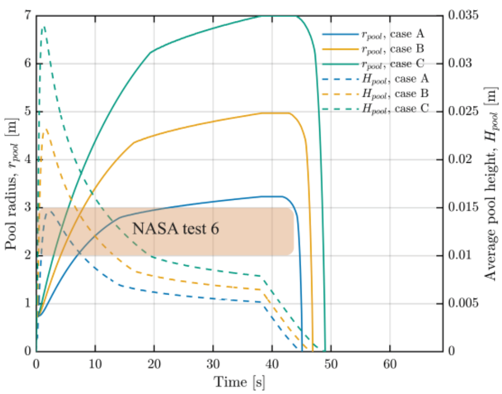

Figure 1. Validation of the pool model with the radius range data of the NASA test 6 (Chirivella and Witcofski 1986), considering three different mass flow rates: case A) $\dot{m}_{LH2} = 9.5$ kg/s; case B) $\dot{m}_{LH2} = 4.75$ kg/s; case C) $\dot{m}_{LH2} = 2$ kg/s.

Figure 3 shows the ground temperature profiles for case C) along the pool radius at different simulation times. The model can calculate the temperature in any ring of the pool and based on the wetting time of the j-th ring, update the local temperature accordingly. The simulation demonstrates that the ground temperature increases towards the edge of the pool since the external rings of the pool are in contact with the liquid for a shorter period of time.

Based on the temperature profiles along the ground, conduction heat fluxes were calculated in the j-th ring, thereby enabling the calculation of the local heat balance, the calculation of the evaporated mass, and finally the local mass balance. The cumulative evaporated mass per ring over the simulation is highlighted in Figure 4. The figure shows the radial distribution of the cumulative evaporated mass $m_{EV,\,tot\,(r,\,t)}$ along the radius of the pool for different instants.

The evaporated mass peaks in an intermediate region of the radius, decreasing towards both the pool center and the outer edge of the pool.

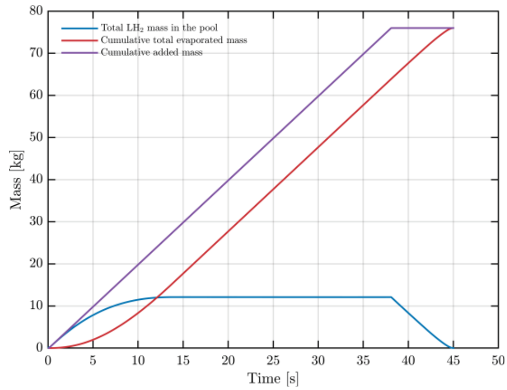

Figure 2. Pool mass evolution over time for case C) $\dot{m}_{LH2} = 2$ kg/s.

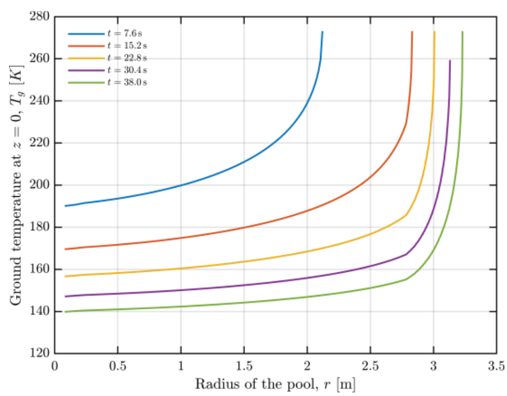

Figure 3. Ground temperature profiles $T_g(0, t)$ along the radius *at different times* for case C) $\dot{m}_{LH2} = 2$ kg/s.

This behavior reflects the balance between the temporal evolution of the local heat flux and the effective area of the rings. On one hand, the central rings, although exposed for longer to local heat flux, contribute with a reduced area compared to the outer rings. Additionally, the longer the exposure to LH_2, the lower the ground temperature beneath the pool, leading to a reduced heat flux over time. On the other hand, peripheral rings, although characterized by a larger area, are exposed for a shorter time to heat flux due to the spreading (or reduction) of the pool. The intermediate region maximizes the product of exposure time and evaporating surface area, resulting in the maximum cumulative evaporated mass.

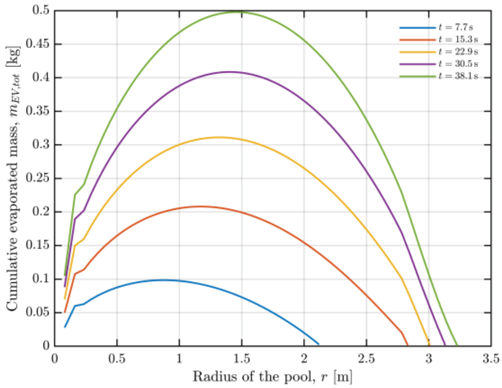

Figure 4. Cumulative evaporated mass $m_{\mathrm{EV,tot}}$ (r, t) per ring at selected times along the radius for case C) $\dot{m}_{LH2} = 2$ kg/s.

4. Discussion

The good agreement of the evaporation time after valve shut-off for case C) (see Figure 1) proves that the ring reduction model is a very precise way to simulate pool evaporation phenomena. Current models that use a constant pool height during reduction may lack accuracy because, as the pool shrinks with a constant height, evaporation slows rather than speeds up. However, the smaller the pool (and the radius), the faster the evaporation. This is also evidenced by the work conducted by (Nguyen *et al*. 2024), which points out that in the simulations conducted with a constant height, the cryogenic pools on the ground need more time to evaporate.

The overprediction of the pool radius in Figure 2 is a consequence of different factors. Firstly, the LH_2 evaporation before ground contact is not considered in this study. However, this phenomenon cannot be accurately estimated when simulating the NASA test 6. Notably, outlet nozzle diameter, release height, and nominal pressure at the release valve are unknown. Since the flashing phenomenon after the leak and the droplet size are dependent on the jet velocity and on the thermodynamic properties of the fluid at the nozzle (Rescigno *et al*. 2025), it is not possible to validate all the phenomena from liquid discharge to pool spreading. Thus, only a comparison with the radius range is possible, simulating various mass flow rates.

Grønli *et al.* (Grønli *et al* 2025) simulated NASA test 6 and obtained a maximum pool radius of roughly 5.5 m when using a film boiling regime for the convection term, while they obtained a maximum pool radius of roughly 3.8 m considering a perfect thermal contact between the cryogenic liquid and the ground. The difference in the maximum pool radius with this study (7 m) may be due to the different film boiling regime equations used, which can lead to different heat fluxes. Nonetheless, in their simulations, even with perfect thermal contact, the pool radius is overestimated, suggesting again that flashing after release occurs.

Nevertheless, the perfect thermal contact model tends to overestimate the heat flux when considering cryogenic fluids. The perfect thermal contact model assumes that the ground temperature $T_g(0, t)$ is constantly equal to the cryogenic fluid temperature. However, due to the temperature difference between the ground and the liquid, a gas layer forms between the cryogenic pool and the ground (Shirai *et al.* 2010). However, experiments discussed in (Nguyen *et al.* 2024) revealed that after the discharge of liquid nitrogen, the ground surface temperature almost reached the liquid nitrogen temperature after a few seconds. The results of the experiments show that the temperature of the soil drops immediately and significantly. Therefore, with the current film boiling correlations, it is not possible to model the phenomenon accurately. Thus, the actual behavior may lie somewhere between perfect thermal contact and the film boiling regime.

This study warns that in the region immediately downstream of the source, a stable boiling regime cannot be achieved throughout the release phase, as the cryogenic fluid droplets continuously impact the ground. In areas outside the impact area, the liquid moves by gravity and will therefore continuously break the thin gas layer that forms as soon as the liquid touches the ground. Before boiling occurs, nucleation and phase transition take place. However, with current mathematical correlations that assign the regime based on the temperature difference between the ground and the fluid, the boiling regime is always assigned for LH_2 without first considering nucleation and transition. This, therefore, could limit heat flux when studying a fluid in motion and not in a stable scenario, e.g., a tank containing liquid hydrogen, as in (Ustolin *et al*. 2021).

5. Conclusion

This study developed and validated a novel ring reduction model to simulate the spread and evaporation of cryogenic pools, particularly for LH_2. The methodology simulates the spreading and contraction of the pool by adding or removing concentric rings based on local mass and energy balances. The model showed good agreement with the evaporation time observed in NASA test 6. However, the pool radius was overestimated, mainly due to unmodelled pre-impact evaporation (flashing after discharge and droplet evaporation) from unknown release conditions. The model calculates the temporal evolution of the ground temperature beneath the pool. The results indicate that the ground temperature increases towards the edge of the pool. Furthermore, the analysis highlights a crucial limitation of the current heat transfer correlations when simulating the spreading of a pool. The choice between the use of i) correlations for film boiling or ii) the classical assumption of perfect thermal contact appears to be still a research gap. Experimental evidence suggests that the actual pool behavior lies somewhere in between. Perfect thermal contact overestimates the heat flux, while correlations for film boiling underestimate it and may not be fully applicable during the spreading phase. Therefore, future work will be carried out to i) compare the ring reduction model with other methods and ii) focus on the development and implementation of new heat transfer correlations specifically designed for forced convection and spreading cryogenic fluids to improve the accuracy of predictions for dynamic pool scenarios.

Acknowledgement

This work is conducted with the support of the HYDROGENi Research Centre (Grant No. 333118), funded by industrial partners and the Research Council of Norway under the Norwegian research program FMETEKN. Furthermore, this work was undertaken as part of the ELVHYS project No. 101101381 supported by the Clean Hydrogen Partnership and its members and the European Union. UK participants in Horizon Europe Project ELVHYS are supported by UKRI grant numbers 10063519 (University of Ulster) and 10070592 (Health and Safety Executive), funded by the European Union. Views and opinions expressed are however, those of the author(s) only and do not necessarily reflect those of the European Union or Clean Hydrogen JU. Neither the European Union nor the granting authority can be held responsible for them.

References

Baldwin, Michael, Ali Ghavami, S. Mostafa Ghiaasiaan, and Alok Majumdar. 2021. "Pool Boiling in Liquid Hydrogen, Liquid Methane and Liquid Oxygen: A Review of Available Data and Predictive Tools." *Cryogenics* 115 (December 2020): 103240. https://doi.org/10.1016/j.cryogenics.2020.103240.

Bell, Ian H., Jorrit Wronski, Sylvain Quoilin, and Vincent Lemort. 2014. "Pure and Pseudo-Pure Fluid Thermophysical Property Evaluation and the Open-Source Thermophysical Property Library CoolProp." *Industrial & Engineering Chemistry Research* 53:2498–2508. https://doi.org/doi:10.1021/ie4033999.

Bergman, Theodore L., and Adrienne S. Lavine. 2018. *Fundamentals of Heat and Mass Transfer*. Eighth.

Breen, B., and J. Westwater. 1962. "Effect of Diameter of Horizontal Tubes on Film Boiling Heat Transfer." *Chemical Engineering Progress* 58:67–72.

Chirivella, J.E., and R.D. Witcofski. 1986. "Experimental Results from Fast 1500-Gallon LH2 Spills." *Am Inst Chem Eng Symp Ser* Vol. 82 (251).

Goff, Richard, Andrew Newton, Greg Wray, Wayne Rattigan, Janni Vizma, and Kieran Lyons. 2024. "Failure of the Vacuum in a Vacuum Insulated Hose While Flowing Liquid Hydrogen." *Institution of Chemical Engineers Symposium Series* 2024-Novem (171).

Grønli, Martin Spillum, Hans Langva Skarsvåg, and Svend Tollak Munkejord. 2025. "Effect of Substrate Thermal Properties on Evaporating Liquid Hydrogen and Ammonia Spills." *Journal of Loss Prevention in the Process Industries* 97 (April): 105685. https://doi.org/10.1016/j.jlp.2025.105685.

Hall, J. E., P. Hooker, and D. Willoughby. 2014.

"Ignited Releases of Liquid Hydrogen: Safety Considerations of Thermal and Overpressure Effects." In *International Journal of Hydrogen Energy*, 39:20547–53. Elsevier Ltd. https://doi.org/10.1016/j.ijhydene.2014.05.141.

Holborn, P G, J M Ingram, and CB Benson. 2022. "Modelling Studies of the Hazards Posed by Liquid Hydrogen Use in Civil Aviation." *IOP Conference Series: Materials Science and Engineering* 1226 (1): 012059. https://doi.org/10.1088/1757-899x/1226/1/012059.

Jin, Tao, Mengxi Wu, Yuanliang Liu, Gang Lei, Hong Chen, and Yuqi Lan. 2017. "CFD Modeling and Analysis of the Influence Factors of Liquid Hydrogen Spills in Open Environment." *International Journal of Hydrogen Energy* 42 (1): 732–39. https://doi.org/10.1016/j.ijhydene.2016.10.162.

Nguyen, Le-duy, Myungbae Kim, Yongshik Han, and Kyuhyung Do. 2024. "A Large-Scale-Outdoor Continuous Release of Cryogenic Liquid onto Ground" 191 (September): 1565–79.

Rescigno, Davide, Alessandro Campari, Alexandros G. Venetsanos, and Federico Ustolin. 2025. "Modeling of Accidental Liquid Hydrogen Spills and Rainout." In , edited by ESREL SRA-E 2025, 1957–64. Research Publishing, Singapore. https://doi.org/10.3850/978-981-94-3281-3.

Shirai, Yasuyuki, Hideki Tatsumoto, Masahiro Shiotsu, Koichi Hata, Hiroaki Kobayashi, Yoshihiro Naruo, and Yoshifumi Inatani. 2010. "Boiling Heat Transfer from a Horizontal Flat Plate in a Pool of Liquid Hydrogen." *Cryogenics* 50 (6–7): 410–16. https://doi.org/10.1016/j.cryogenics.2010.04.001.

TNO. 2005. *Yellow Book - Methods for the Calculation of Physical Effects Due to Releases of Hazardous Materials (Liquids and Gases)*. Edited by R.A.P.M. Weterings C.J.H. van den BOSCH. Third edit. The Hague.

Ustolin, Federico, Federica Ferrari, and Nicola Paltrinieri. 2022. "Prediction of Condensed Phase Formation during an Accidental Release of Liquid Hydrogen." *Chemical Engineering Transactions* 91:439–44. https://doi.org/10.3303/CET2291074.

Ustolin, Federico, Tommaso Iannaccone, Valerio Cozzani, Sepideh Jafarzadeh, and Nicola Paltrinieri. 2021. "Time to Failure Estimation of Cryogenic Liquefied Tanks Exposed to a Fire." In *Proceedings of the 31st European Safety and Reliability Conference, ESREL 2021*, 935–42. Research Publishing, Singapore. https://doi.org/10.3850/978-981-18-2016-8_182-cd.

Verfondern, K., and B. Dienhart. 2007. "Pool Spreading and Vaporization of Liquid Hydrogen." *International Journal of Hydrogen Energy* 32 (13): 2106–17. https://doi.org/10.1016/j.ijhydene.2007.04.015.

Wang, Lei, Yanzhong Li, Feini Zhang, Fushou Xie, and Yuan Ma. 2016. "Correlations for Calculating Heat Transfer of Hydrogen Pool Boiling." *International Journal of Hydrogen Energy* 41 (38): 17118–31. https://doi.org/10.1016/j.ijhydene.2016.06.254.

Webber, D. M. 1990. "Model for Pool Spreading and Vaporisation and Its Implementation in the Computer Code GASP."

Witlox, H. 2000. "Model for Pool Spreading, Evaporation and Solution on Land and Water (PVAP) – Theory Manual, Consequence Modeling Documentation (PHAST Technical Reference)."

Witlox, H, A.O. Oke, and M. Fernandez. 2023. "Theory - Pool Vaporisation."